NASA TECHNICAL MEMORANDUM 89033

FACTORS INFLUENCING ELASTIC STRESSES IN DOUBLE CANTILEVER BEAM SPECIMENS

J. H. Crews, Jr., K. N. Shivakumar

and I. S. Raju

NOVEMBER 1986

NASA
National Aeronautics and
Space Administration

Langley Research Center
Hampton, Virginia 23665

INTRODUCTION

The double cantilever beam specimen is widely used for fracture toughness testing. Although first introduced to evaluate adhesives, it has more recently become popular for opening-mode (mode I) delamination testing of laminated composites. Adhesive tests often involve aluminum adherends and a debond-starter insert at the loaded end of the specimen. For composite testing, unidirectional (0° plies) are usually co-cured with the starter insert located at the specimen midplane. Questions often arise when comparing double cantilever beam (DCB) specimen results from different sources because of the different adherend materials used or because of differences in adherend or adhesive thicknesses. Several test programs have shown that specimen parameters can influence fracture toughness measurements (refs. 1 and 2). Similarly, analyses have shown that specimen parameters can influence the local stress distributions around the delamination front (ref. 3).

The present research was inspired by these earlier studies, which emphasized the need for a better understanding of the DCB specimen. The objective of the present study was to identify DCB specimen parameters that influence the stress distributions ahead of the delamination. Emphasis was placed on analyzing stress distributions rather than stress intensity factors since DCB specimens with the same stress distribution shape but with different stress intensity factors should produce the same toughness value. On the other hand, different stress distribution shapes can produce different amounts of yielding ahead of the delamination and this may influence interlaminar toughness.

A two-dimensional elastic stress analysis was conducted using a finite-element model of a DCB specimen. The adhesive bondline as well as the adherends were modeled. The model had a very high mesh refinement in the

adhesive near the delamination and had singularity elements at the delamination tip. The specimen dimensions were typical of currently used DCB specimens. This study focused on an aluminum DCB specimen and a graphite/epoxy DCB specimen. Adhesive thicknesses were varied from that of co-cured laminates to that of thick adhesive bondlines. In addition, the adherend thickness and stiffness were studied for typical values as well as for several extreme values. An all-resin DCB specimen without a bondline was also analyzed as a monolithic reference case.

Results were presented as stress distributions for the local region ahead of the delamination tip. These DCB stress distributions were compared with one another and also with a monolithic reference case. The stress distributions were used to estimate the extent of yielding ahead of a propagating delamination. The yield zone sizes were estimated for a range of adhesive thicknesses. Finally, the yield zone areas and heights were used in a general discussion of interlaminar fracture toughness.

SYMBOLS

a	delamination length, m
D	flexural stiffness, Nm
E_L	Young's modulus in longitudinal direction, GPa
E_T	Young's modulus in transverse (thickness) direction, GPa
G_I	strain energy release rate, J/m^2
G_{Ic}	fracture toughness, J/m^2
G_{LT}	shear modulus in longitudinal-transverse plane, GPa
h	adherend thickness, m
K_I	stress intensity factor (mode I), $N/m^{3/2}$
K_{Ic}	critical K_I, $N/m^{3/2}$

P	applied load, N/m
t	adhesive thickness, m
x,y	Cartesian coordinates, m
Δ	length of singularity element, m
ν_{LT}	Poisson's ratio
σ_x	normal stress in x-direction, MPa
σ_y	normal stress in y-direction, MPa
σ_{yld}	adhesive yield stress, MPa
τ_{xy}	shear stress in x-y plane, MPa

FINITE ELEMENT ANALYSIS

Figure 1 shows the DCB specimen configuration and loading analyzed in this study. As previously mentioned, the specimen dimensions and materials were selected to represent those typical of currently used test specimens. Notice that h represents the thickness of each adherend; whereas, t represents the total thickness of the adhesive layer. The delamination was assumed to be symmetrically located at the center of this adhesive layer. For convenience, the delamination tip will be called a crack tip. For all cases, a 50 mm delamination length was used and the coordinate origin was located at the crack tip, as shown. The adhesive properties used throughout this study were typical of a brittle epoxy. These material properties as well as the adherend properties are shown in Table 1.

Because of midplane symmetry, only the upper half of the DCB specimen was modeled in the finite element analyses. The model was constrained to produce plane strain conditions. The region near the delamination tip is shown in figure 2. This two-dimensional model consists of eight-noded, parabolic elements. The enlarged portions of the model show the mesh refinement in the

adhesive near the delamination tip. At the delamination tip, quarter-point singularity elements in the form of triangles (ref. 4, 5, and 6) were used. The singularity element size Δ was equal to 0.00002 mm. The polar mesh arrangement near the crack tip was expected to produce an accurate representation of the crack-tip stress field. The entire finite element model had 520 elements with 1667 nodes. The model was expected to produce accurate stress distributions throughout the DCB specimen. The stresses were calculated at nodal points.

The strain energy release rate for delamination growth was calculated using the virtual crack closure technique (ref. 7), which involves the forces ahead of the crack tip and the displacements behind the crack tip. Referring to the quarter-point singularity elements in figure 2, the strain energy release rate is obtained as (ref. 8)

$$G_I = -\frac{1}{2\Delta}\left[F_{yi}\left\{ \frac{12 - 3\pi}{2}(v_m - v_{m'}) + (6\pi - 20)(v_l - v_{l'})\right\}\right.$$

$$\left. + F_{yj}\left\{ \frac{v_m - v_{m'}}{2} + v_l - v_{l'},\right\}\right] \qquad (1)$$

where F_{yi} and F_{yj} are the forces in the y-direction at nodes i and j. The terms $v_m - v_{m'}$ and $v_l - v_{l'}$ are the relative displacements between nodes m and m' and between l and l', respectively. Note that the nodes j and l are the quarter-point nodes.

The stress intensity factors can be computed from

$$K_I = \sqrt{EG_I/(1 - \nu^2)} \qquad (2)$$

where E and ν are the Young's modulus and Poisson's ratio of the adhesive.

RESULTS AND DISCUSSION

The results are presented in three sections. First, results are presented for an aluminum DCB specimen. The finite element model was evaluated by comparing the stress distributions and stress intensity factors for the aluminum DCB specimen with known solutions for a monolithic case. Next, the stress distributions ahead of the crack are analyzed for a range of DCB specimen parameters using the graphite/epoxy specimen. Finally, these elastic stresses are used to estimate yielding near the crack tip.

Aluminum DCB Specimen

Figure 3 shows the σ_x and σ_y distributions along the adhesive midplane computed for the aluminum DCB specimen subjected to a unit load. This specimen represents an adhesive bonding case having a typical adhesive thickness of 0.10 mm. Both σ_x and σ_y have peak values at the crack tip ($x = 0$). However, as expected, σ_y is the dominant stress for this opening-mode specimen. Notice that σ_y becomes compressive beyond about 3 mm from the crack tip and gradually decays to zero by about 20 mm. The σ_y integral equals the applied load P. The remainder of this paper will focus on the σ_y distributions and will emphasize the local region very near the crack tip.

The σ_y stress distribution from figure 3 is replotted as the solid curve in figure 4 using log-log coordinates. For comparison, the dashed curve in figure 4 represents the monolithic (all-resin) DCB specimen that was used as a reference case. The upper part of this dashed curve is straight and has the expected -1/2 slope associated with crack singularities. The linear portion of the dashed curve also indicates the stress intensity level for the monolithic case. The corresponding stress intensity factor K_I, calculated directly from the dashed curve, was 370 $N/m^{3/2}$. This agrees with 375.4 $N/m^{3/2}$ calculated using equation (2) and the virtual crack closure technique,

equation (1). Also, the closed-form solution from reference 9 was applicable for this monolithic case and produced a K_I value of 377.1 $N/m^{3/2}$. The accuracy demonstrated for this monolithic case is believed to be representative of the other DCB cases since the same finite-element model and analysis procedures were used throughout this study.

Comparison of the solid curve in figure 4 with the dashed reference curve shows that the aluminum DCB specimen has, as expected, the same stress gradient in the singularity-dominated region. However, the aluminum DCB case has a lower stress intensity factor because its curve is lower. A stress intensity factor of 84.1 $N/m^{3/2}$ was calculated for this aluminum DCB case using the virtual crack closure technique. Stress intensity factors calculated by this technique are given in Table 1 for all cases analyzed. The K_I solution from reference 9 does not apply to the DCB specimen when the adherend and adhesive properties are different.

To estimate the extent of yielding ahead of the crack tip, the loads for the two cases in figure 4 were scaled up to produce a "critical" condition at the crack tip. For each curve, the unit load was multiplied by the ratio K_{Ic}/K_I, where K_{Ic} is the adhesive fracture toughness, 1.18 $MN/m^{3/2}$ (ref. 10). This procedure is based on the simplifying assumption that the crack growth is controlled completely by the elastic K_I level at the crack tip. As a result, when the different cases were scaled up to the same K_{Ic} level, the linear portions of the stress distributions near the crack tip were identical. These scaled curves and the corresponding loads are shown in figure 5. This comparison illustrates a "hump" in the σ_y distribution for the aluminum DCB specimen. In the region 0.1 to 1 mm ahead of the crack tip, the σ_y stresses in the aluminum DCB are about three times higher than those for the monolithic case. The large difference in the Young's moduli for the adherend and

adhesive (71.0 GPa compared to 3.45 GPa) is believed to be responsible for this effect. In reference 3, Wang et al interpreted this effect as a reduction in the size of the singularity-dominated region near the crack. However, the present results suggest that the effect is superposed on the singularity-dominated stress distribution.

Because σ_y is the dominant stress ahead of the crack tip, the scaled σ_y curves in figure 5 were compared with the resin yield stress to estimate the extent of yielding associated with crack growth. The dashed curve exceeds the 44 MPa resin yield stress (ref. 11) for a distance of only about 0.1 mm ahead of the crack tip. In contrast, the elevated stresses for the aluminum DCB case exceed this yield level for about 1 mm. Although the elevated σ_y stresses extend the length of the crack-tip yield zone, the thickness of the adhesive layer limits the height of the zone. These competing influences on the yield-zone area will be discussed in a subsequent section using the von Mises yield criterion. For brittle adhesives, crack growth may produce little plasticity ahead of the crack tip and, therefore, may be controlled entirely by the singularity-dominated region close to the crack tip. For tough adhesives, however, crack growth yields the adhesive well ahead of the crack tip and the size of the plastic zone will be influenced by the elevated σ_y stresses shown in figure 5. The extent of yielding ahead of the crack tip may influence the toughness measurements obtained with DCB specimens. This influence will be discussed later in this paper.

Figure 6 shows the stress distributions along the adherend-adhesive interface near the crack tip. Recall that the crack is located at the adhesive midplane. The σ_x stress in figure 6 acts parallel to the interface; whereas, σ_y and τ_{xy} act on the interface. All three stress components have peaks near the crack-tip region. The shear stress region is rather small and,

as expected, σ_y is the dominant stress component. This elastic σ_y stress exceeds the 44 MPa resin yield strength for a distance of about 1 mm ahead of the crack tip. Also, the high stresses shown in figure 6 could cause an interfacial failure which would shift the crack tip from the adhesive midplane to the interface. Although such interfacial failures are important, they are beyond the scope of the present study.

Graphite/Epoxy DCB Specimen

The graphite/epoxy DCB specimen was modeled using properties for T300/5208, see Table 1. The adherends each represented twelve 0^o plies. The adhesive was 0.01 mm thick, corresponding to a "resin-rich" interface in a co-cured laminate. This case has material properties and dimensions that are typical of current graphite/epoxy specimens and will therefore be used as a reference case for subsequent discussions. The σ_y distribution for this reference case is shown in figure 7, where it is compared with the curves for the aluminum DCB and the monolithic specimens (from figure 5). As in figure 5, all three curves in figure 7 have been scaled up to the critical crack-tip condition for crack growth. The graphite/epoxy curve shows an elevation in the σ_y stresses, like the aluminum specimen, but it is less pronounced and occurs closer to the crack tip. Comparison of the three curves at the resin yield stress (44 MPa) shows that the adhesive in the graphite/epoxy specimen would yield about three times farther in the x-direction than that for monolithic case but only about one-third as far as the aluminum case. The difference in the σ_y distributions can be related to the differences in the elastic properties and specimen dimensions for the graphite and aluminum specimens. In the remainder of this section, the effects of these specimen parameters on the σ_y distribution will be analyzed.

Effects of adhesive thickness.- The effects of adhesive thickness are illustrated in figure 8. Four adhesive thicknesses were used with the same adherend properties and thickness (1.65 mm). As previously mentioned, the curve for t = 0.01 mm represents a co-cured laminate. The curve for t = 0.10 mm represents an adhesively-bonded specimen. Notice that the four curves agree with one another near the crack tip, indicating the same K_I value for all four adhesive thicknesses. This shows that the adhesive thickness has very little influence on the stress intensity factors. However, beyond this very local region near the crack tip, the four curves differ. The σ_y stresses are elevated most for t = 0.01 mm (graphite/epoxy reference case) and have a nearly linear distribution for the extreme case with t = 0.66 mm.

Effects of adherend flexural stiffness.- The effects of adherend thickness are illustrated by figure 9. Recall that for the graphite/epoxy reference case, the 1.65 mm adherend thickness represents 12 graphite/epoxy plies. The h = 2.20 mm and 1.10 mm cases correspond to 16 and 8 plies and have different stress intensity factors. However, the curves for these two cases have been scaled to coincide with the reference curve near the crack tip. The three curves in figure 9 agree with one another over most of the range, showing that, although the adherend thickness influences K_I, it has little influence on the shape of the σ_y distribution for these thin bond line cases. Results in reference 12 showed that adherend thickness had a small effect on the DCB critical strain energy release rate G_{Ic}.

A similar small effect on the shape of the σ_y distributions is shown in figure 10 for a range of adherend stiffnesses. The reference graphite/epoxy case is compared with a similar case that differs only in the value of longitudinal stiffness E_L used. Again, the load for the non-reference case was scaled so that the two curves would agree over their linear portions.

The two comparisons using different adherend thicknesses and moduli from figures 9 and 10 are combined in figure 11. For this figure, the adherend modulus was adjusted for each of the non-reference adherend thicknesses so that all three cases had the same bending stiffness D ($D=E_L h^3/12$). Scaling was not required to produce the nearly perfect agreement between the three curves. This illustrates that specimens with different adherend longitudinal moduli E_L and adherend thicknesses h will have nearly identical σ_y distributions and identical stress intensity factors if they have the same bending stiffness.

Effects of adherend transverse stiffness.- The last specimen parameter investigated was E_T, the transverse stiffness for the adherend. Results for two cases with different E_T values are shown in figure 12. The reference case is compared with a similar case differing only in the E_T value used. The two cases had the same stress intensity factor. The higher value of E_T produced significantly higher σ_y values beyond the linear portions of these curves. Because the higher E_T value used in figure 12 is rather extreme, a second comparison was made. Figure 13 shows the reference case again but compares it with an aluminum DCB specimen having the same adhesive thickness and bending stiffness. Based on the previously discussed comparisons, the difference between these two curves in figure 13 was attributed mostly to their different E_T values. The aluminum DCB specimen has an E_T that is about five times that for the graphite/epoxy reference case. This difference produced σ_y levels in the region of the hump that were twice as large as the reference case.

The characteristic hump in the σ_y distribution appears to be influenced by the adherend stiffness in the thickness direction and does not seem to be influenced by the adherend stiffness in the longitudinal direction. This may

be an important consideration when comparing DCB test results obtained using different adherends.

Yield Zone Estimates

Several studies have shown that adhesive thickness influences G_{Ic} measurements made with DCB specimens (for example ref. 1 and 10). To investigate this influence, adhesive yield zones were estimated for a range of adhesive thicknesses in aluminum specimens. The local stresses corresponded to critical conditions at the crack tip (K_I = 1.18 MN/m$^{3/2}$). Yielding was calculated using the 44 MPa adhesive yield stress with the von Mises yield criterion. Figure 14 presents sketches of the estimated yield zones for six of the adhesive thicknesses. These sketches represent the upper half of the yield zone. As expected, figure 14(a) shows that yielding developed completely through the adhesive for the 0.01 mm case. The zone for this case is quite elongated, having a length of about 15 times the adhesive thickness. For the 0.10 mm case, a typical adhesive bond thickness, yielding also extended to the adherend-adhesive interface but the yield zone length is only about 2.5 times the adhesive thickness. The next case of t = 0.36 mm corresponds to a thick adhesive bond. Yielding extends to the interface and the yield zone is nearly square. For the 0.36 mm case, the yield zone has the largest height but does not extend to the interface. For even larger values of t, the yield zones become smaller.

The yield zone areas and heights are plotted in figure 15 for the full range of adhesive thicknesses investigated. The zone areas increase abruptly with adhesive thickness and reach a maximum near t = 0.3 mm. For larger t values, the areas decrease and appear to approach a limit. This trend in the plastic zone areas agrees qualitatively with the observation that G_{Ic} has a peak level for increasing values of adhesive thickness. However, as

discussed in reference 13, the plastic zone area should correlate better with the plastic energy dissipation associated with loading the specimen up to the critical condition rather than with the energy dissipation during crack growth. As the crack grows, the active plastic zone may simply translate by the amount of crack growth. The plastic energy dissipation associated with an increment of crack growth should be related to the volume of "new" material that yields ahead of the plastic zone as it moves. This volume is proportional to the plastic zone height. The lower curve in figure 15 shows the calculated plastic zone heights. Although less pronounced, the zone-height curve also has a peak like that shown for the zone-size curve. The elastoplastic analysis in reference 13 for a compact tension specimen shows that the plastic energy dissipation during crack growth correlated quite well with plastic zone height but correlated poorly with zone size. Additional insight regarding the DCB plastic zone area and height could be provided by an elastoplastic analysis of crack growth similar to that in reference 13.

CONCLUDING REMARKS

An elastic stress analysis was conducted for a double cantilever beam (DCB) specimen, using two-dimensional finite-element methods. This analysis accounted for orthotropic adherend properties, the adhesive layer between the adherends, and the singularity at the delamination tip. The purpose of this study was to identify the important parameters that influence the stresses near the crack tip. The study focused on an aluminum DCB specimen, typical of adhesively-bonded joints, and on a graphite/epoxy specimen representing a co-cured composite. Opening-mode σ_y stresses ahead of the crack were calculated and compared with similar stresses for a monolithic reference specimen.

In the singularity-dominated region very near the crack tip, the σ_y distribution for the DCB specimen had the same slope as the opening-mode stresses for the monolithic specimen. However, beyond this localized region, the shapes of the σ_y distributions were different; stresses for the DCB specimen were about twice as large as those for the monolithic reference case. This elevation of the σ_y stresses can extend the yield zone to significant distances ahead of a propagating crack.

Several parameters influenced the σ_y stresses ahead of the crack. Thin adhesive layers caused a pronounced σ_y elevation, but for thick adhesive layers this influence virtually disappeared. For thin bondlines, both the thickness and longitudinal stiffness of the adherend influenced the crack-tip stress level, but they had very little influence on the shape of the stress distribution. Therefore, adherend thickness and longitudinal stiffness should have little influence on interlaminar toughness measurements. Specimens with the same bending stiffness had nearly identical σ_y distributions. Although the transverse stiffness of the adherend had no influence on crack-tip stress intensity, it had a significant effect on the stress distribution beyond the singularity-dominated crack-tip region.

Estimates for adhesive yielding beyond the aluminum DCB crack tip showed that both the plastic zone area and zone height increased to a peak value for increasing adhesive thicknesses. These results agree qualitatively with the observed trend for interlaminar toughness measurements over a range of adhesive thicknesses.

Results from this study should contribute to the general understanding of the DCB test specimen. The present results provide insight about which specimen parameters influence the crack-tip stresses and, therefore, should

prove useful for designing new DCB test specimens and when comparing data from different DCB specimens.

REFERENCES

1. Bascom, W. D.; Cottingham, R. L.; Jones, R. L.; and Peyser, P.: The Fracture of Epoxy- and Elastomer-Modified Epoxy Polymers in Bulk and Adhesives. J. of Applied Polymer Science, vol. 19, 1975, pp. 2545-2562.

2. Mangalgiri, P. D.; Johnson, W. S.; and Everett, R. A., Jr.: Effect of Adherend Thickness and Mixed-Mode Loading on Debond Growth in Adhesively Bonded Composite Joints. NASA TM-88992, August 1986.

3. Wang, S. S.; Mandell, J. F.; and McGarry, F. J.: An Analysis of the Crack Tip Stress Field in DCB Adhesive Fracture Specimens. International Journal of Fracture, vol. 14, no. 1, Feb. 1978, pp. 39-58.

4. Barsoum, R. S.: Application of Quadratic Isoparametric Finite Elements in Linear Fracture Mechanics. Int. J. Fracture, vol. 10, 1974, pp. 603-605.

5. Henshell, R. D.; and Shaw, K. G.: Crack Tip Finite Elements Are Unnecessary. Int. J. of Numerical Methods in Engineering, vol. 9, 1975, pp. 496-507.

6. Barsoum, R. S.: On the Use of Isoparametric Finite Elements in Linear Fracture Mechanics. Int. J. of Numerical Methods in Engineering, vol. 10, 1976, pp. 25-37.

7. Rybicki, E. F.; and Kanninen, M. F.: A Finite Element Calculation of Stress Intensity Factors by a Modified Crack Closure Integral. Engr. Fracture Mechanics, vol. 9, 1977, pp. 931-938.

8. Raju, I. S.: Simple Formulas for Strain-Energy Release Rate with Higher Order and Singular Elements. NASA CR-178186, 1986.

9. Fichter, W. B.: The Stress Intensity Factor for the Double Cantilever Beam. Int. J. of Fracture, vol. 22, 1983, pp. 133-143.

10. Chai, H.: Bond Thickness in Adhesive Joints and Its Significance for Mode I Interlaminar Fracture of Composites. Composite Materials: Testing and Design (Seventh Conference), ASTM STP 893, J. M. Whitney, Ed. American Society for Testing and Materials, Philadelphia, 1986, pp. 209-231.

11. Palmer, R. J.: Investigation of the Effect of Resin Material on Impact Damage to Graphite/Epoxy Composites. NASA CR-165677, March 1981.

12. Devitt, D. F.; Schapery, R. A.; and Bradley, W. L.: A Method for Determining the Mode I Delamination Fracture Toughness of Elastic and Viscoelastic Composite Materials. J. Composite Materials, vol. 14, October 1980, pp. 270-285.

13. Shivakumar, K. N.; and Crews, J. H., Jr.: Energy Dissipation Associated with Crack Extension in an Elastic-Plastic Material. Presented at AIAA/ASM/ASCE 26th Structural Dynamics and Materials Conference, San Antonio, TX, May 19-21, 1986. (Also NASA TM-89032, September 1986)

Table 1 - Material Properties and Stress-Intensity Factors

Adherend						Adhesive thickness	
Material	E_L (GPa)	E_T (GPa)	G_{LT} (GPa)	ν_{LT}	h (mm)	t (mm)	$K_I^{(a)}$ ($N/m^{3/2}$)
Aluminum	71.0	71.0	27.3	0.30	6.35 2.05	0.10 0.01	84.1 446.3
Graphite/ Epoxy	134	13.0	6.41	0.34	1.10 1.65 1.65 1.65 1.65 2.20	0.01 0.01 0.05 0.10 0.66 0.01	806.2 446.3 448.1 448.3 442.5 294.8
Special Orthotropic Cases	13.0 56.5 452 134	13.0 13.0 13.0 134	6.41 6.41 6.41 6.41	0.34 0.34 0.34 0.34	1.65 2.20 1.10 1.65	0.01 0.01 0.01 0.01	1387.4 443.2 453.1 433.3
Resin	3.45	3.45	1.33	0.30	6.35	0.01	375.4

(a) Calculated for DCB with a = 50 mm, P = 1 N/m

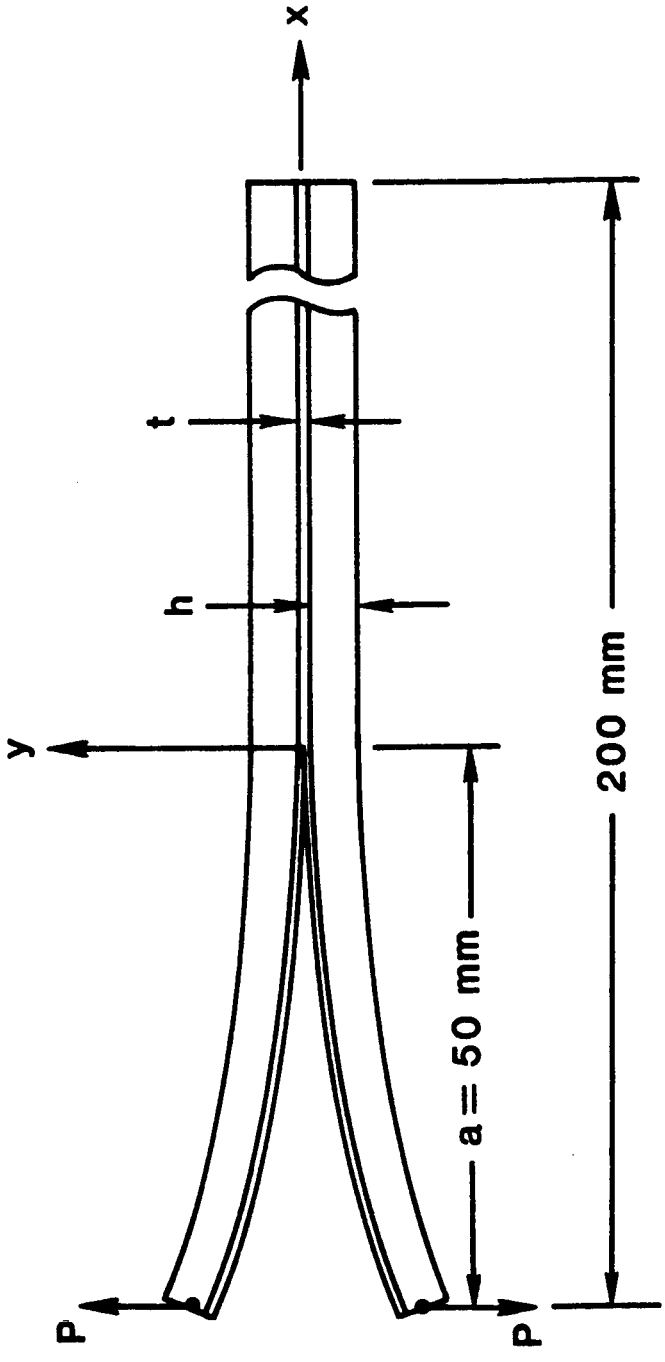

Figure 1.- Double cantilever beam specimen configuration and loading.

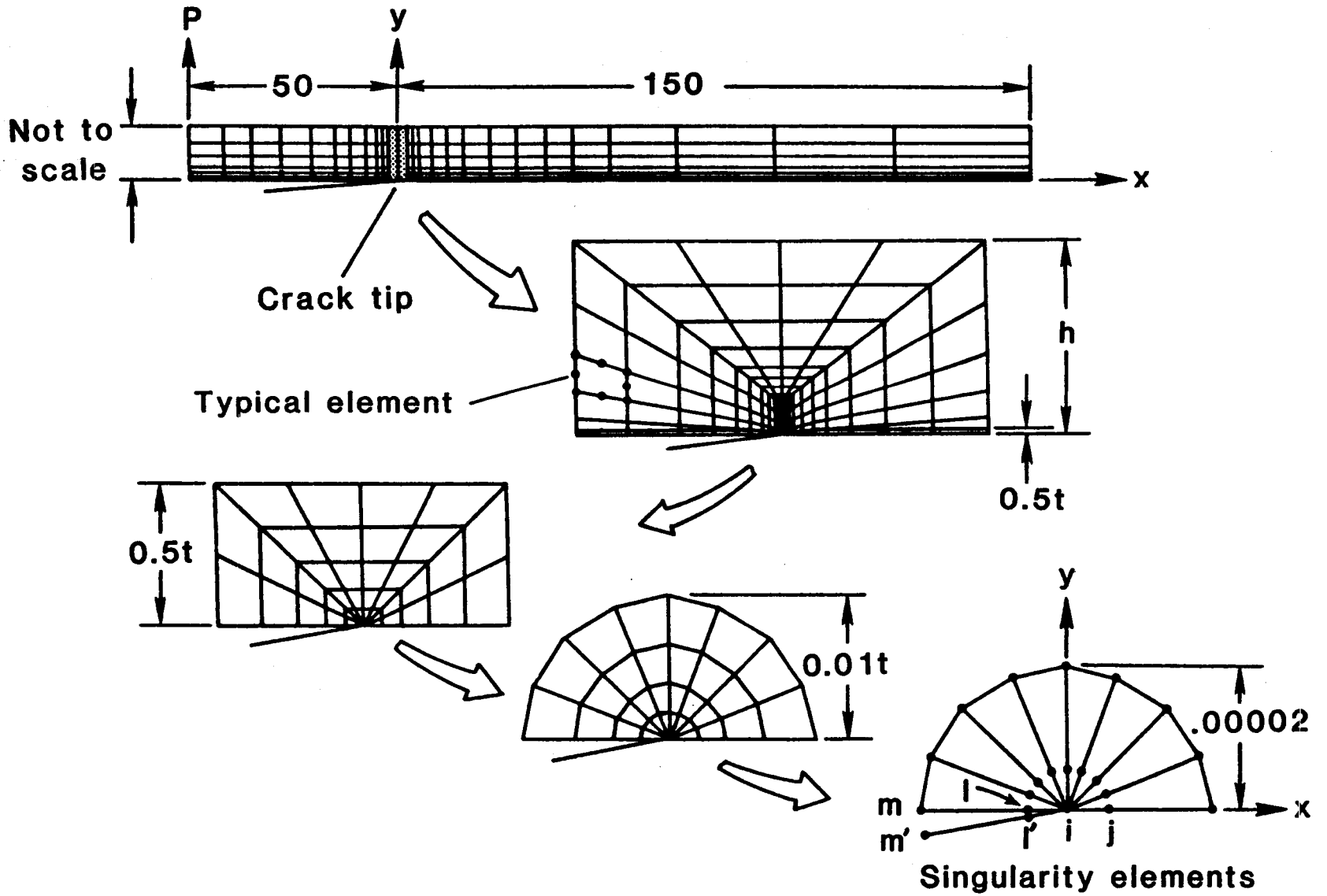

Figure 2.- Finite-element modeling.

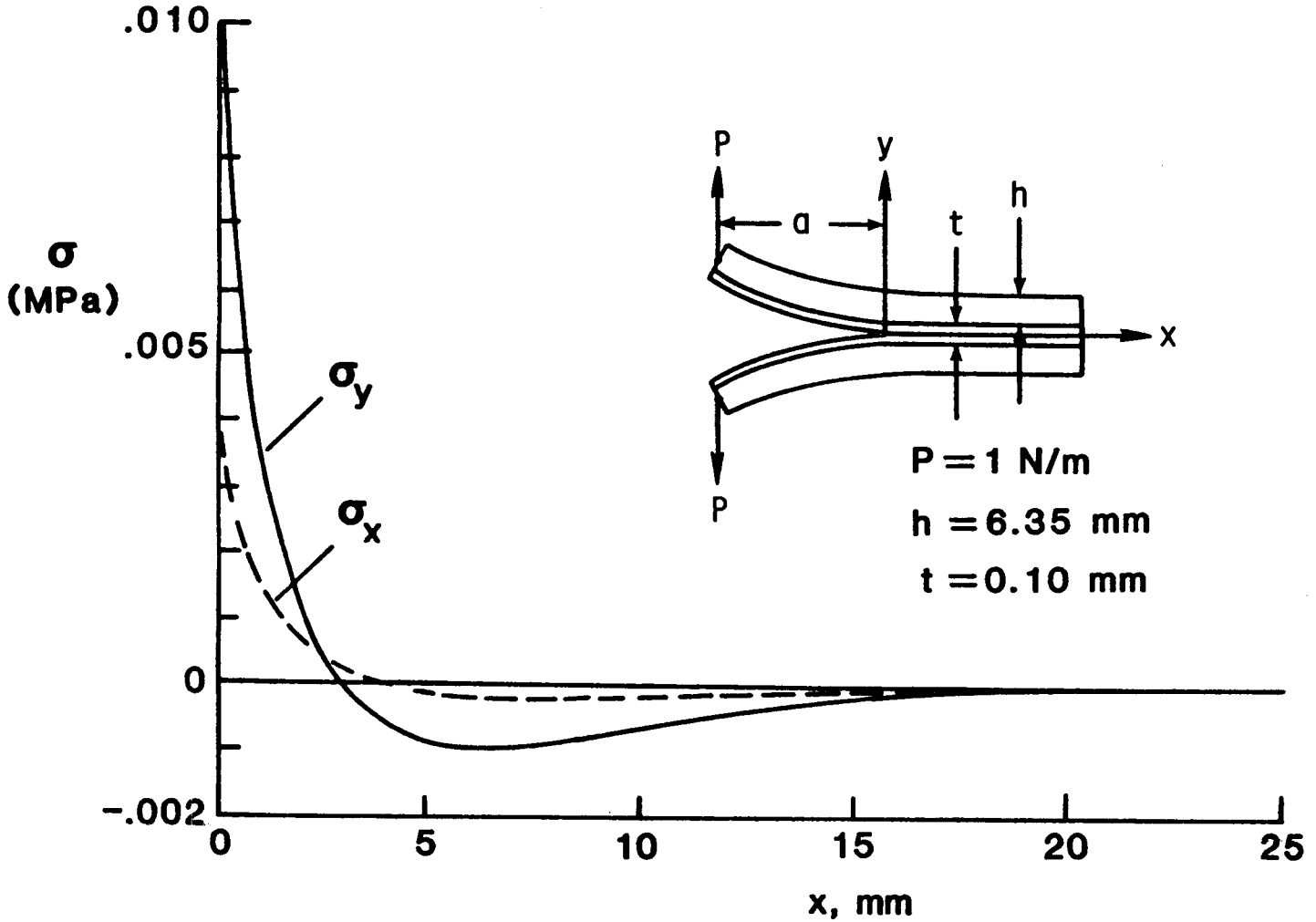

Figure 3.- Stress distributions ahead of delamination in aluminum DCB.

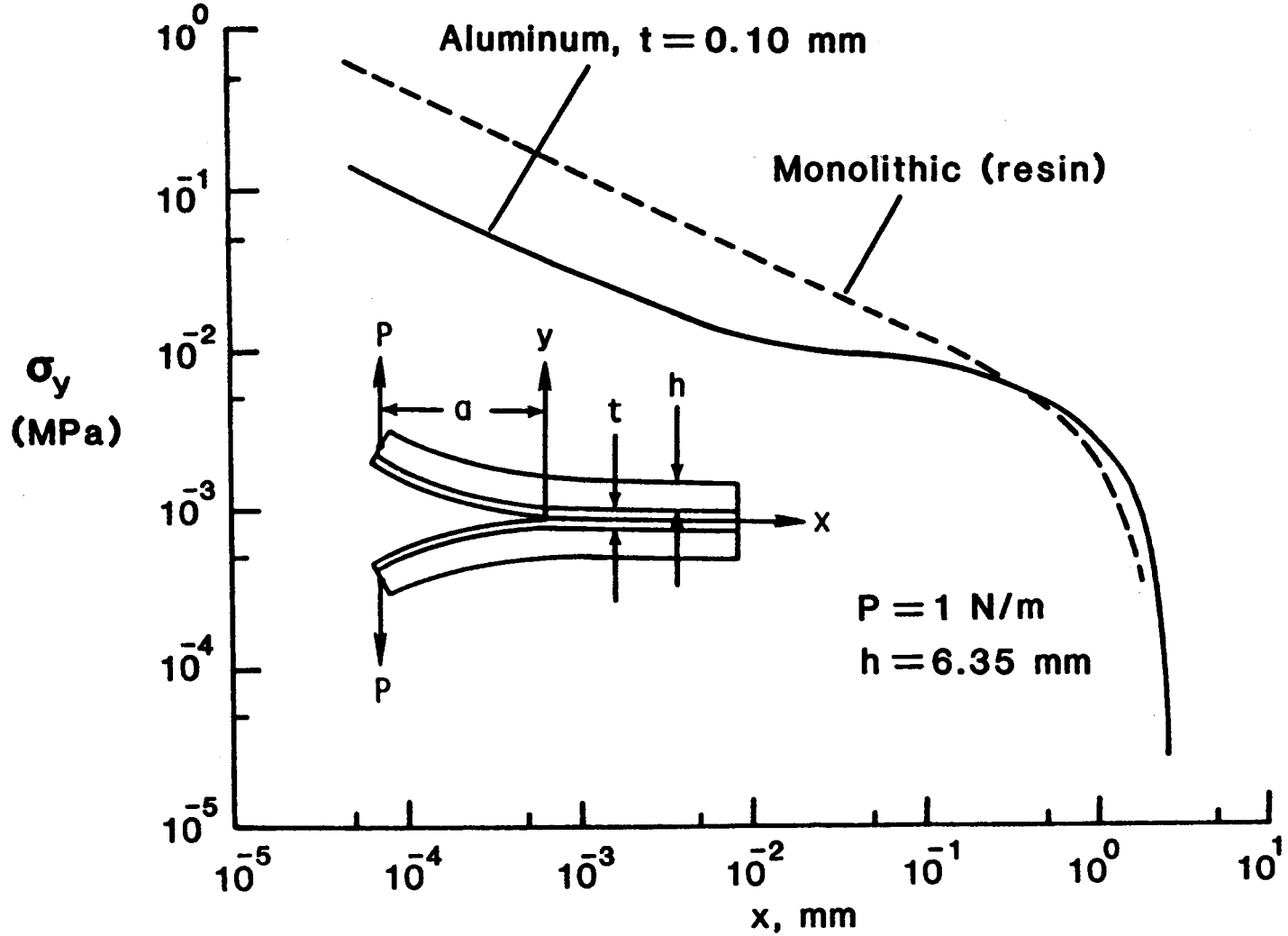

Figure 4.- Distribution of σ_y ahead of crack tip in aluminum DCB.

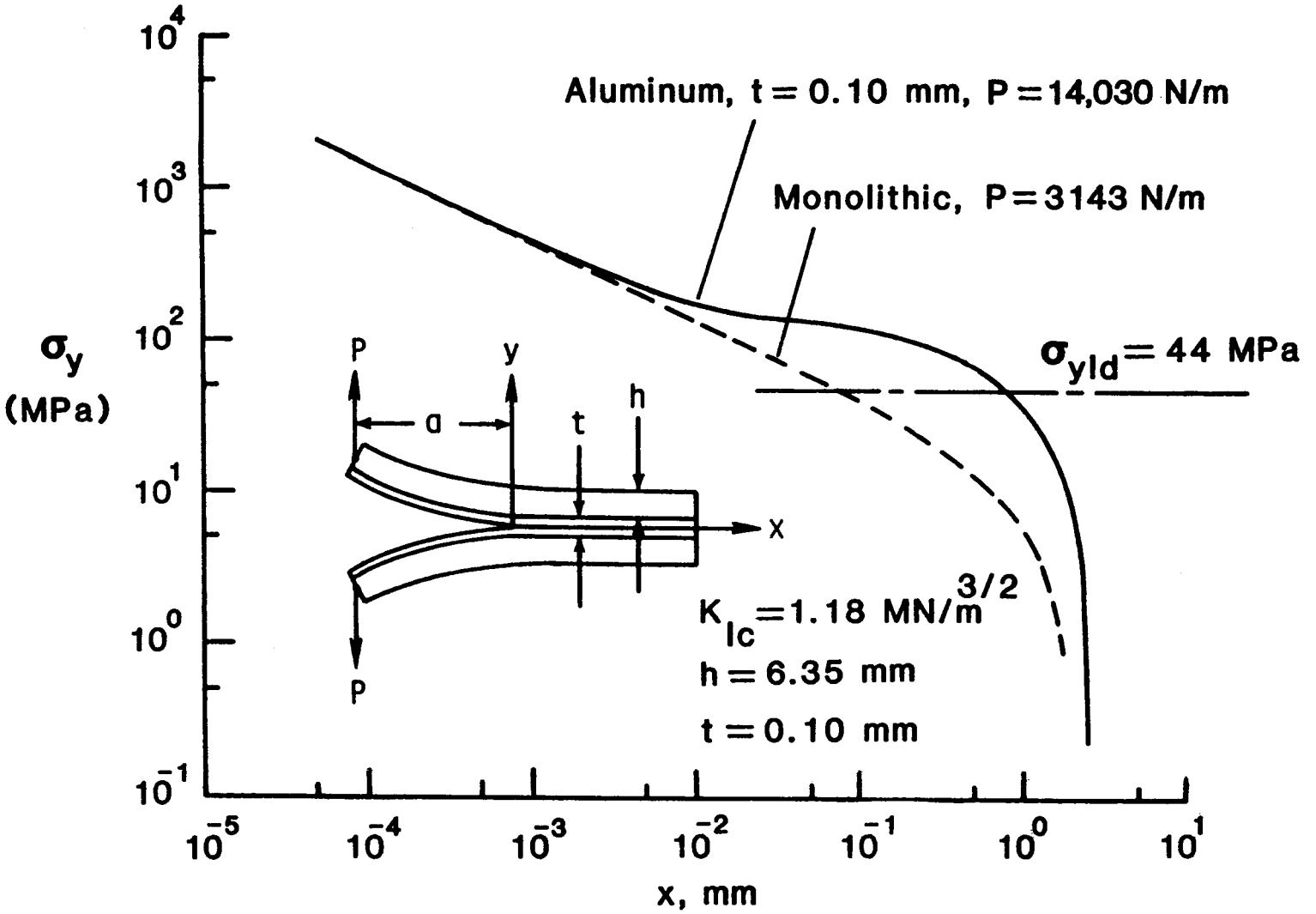

Figure 5.- Distribution of σ_y for aluminum DCB and monolithic specimens.

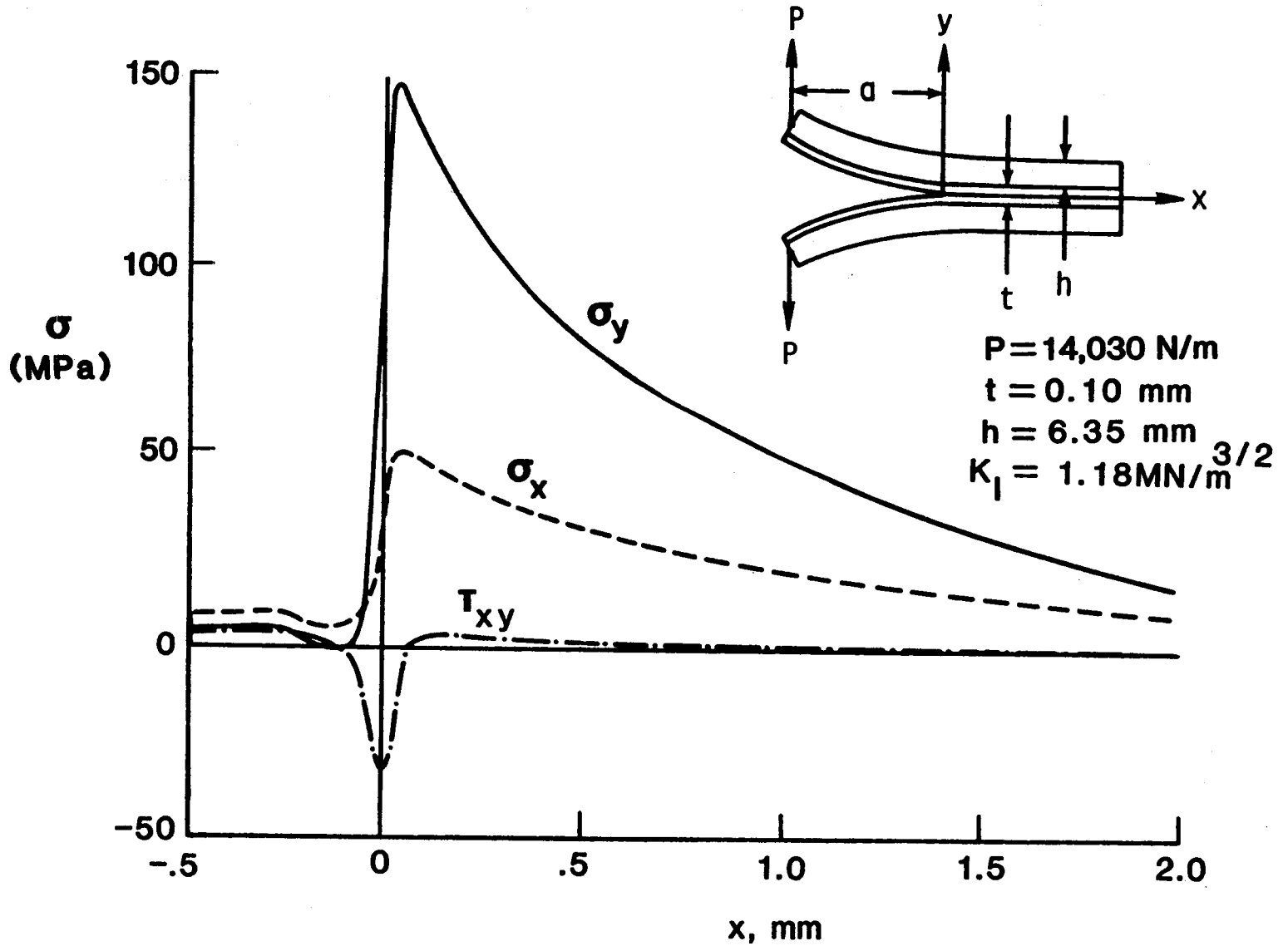

Figure 6.- Interface stress distributions in resin for aluminum DCB.

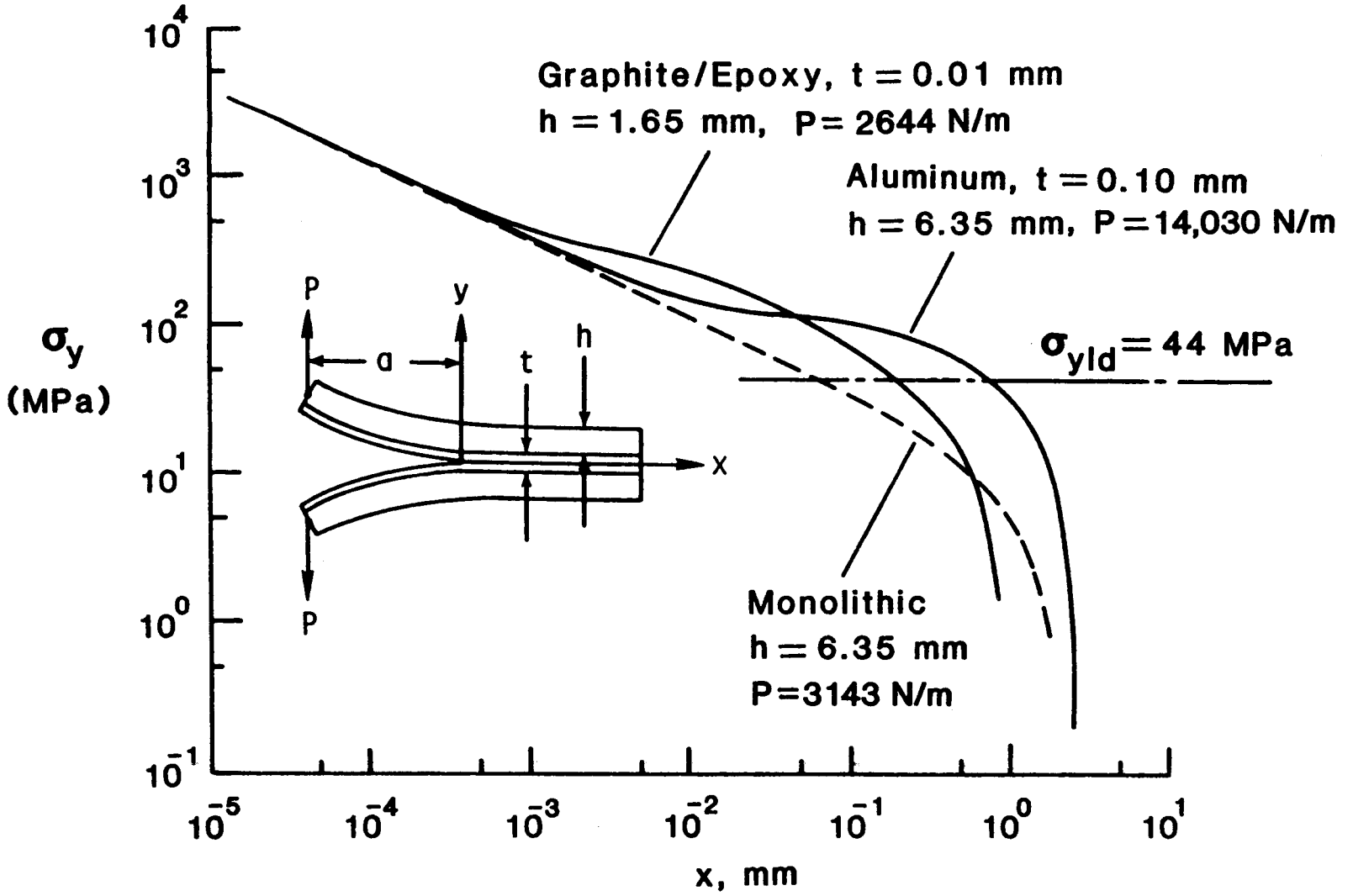

Figure 7.- Comparison of aluminum and graphite/epoxy DCB specimens.

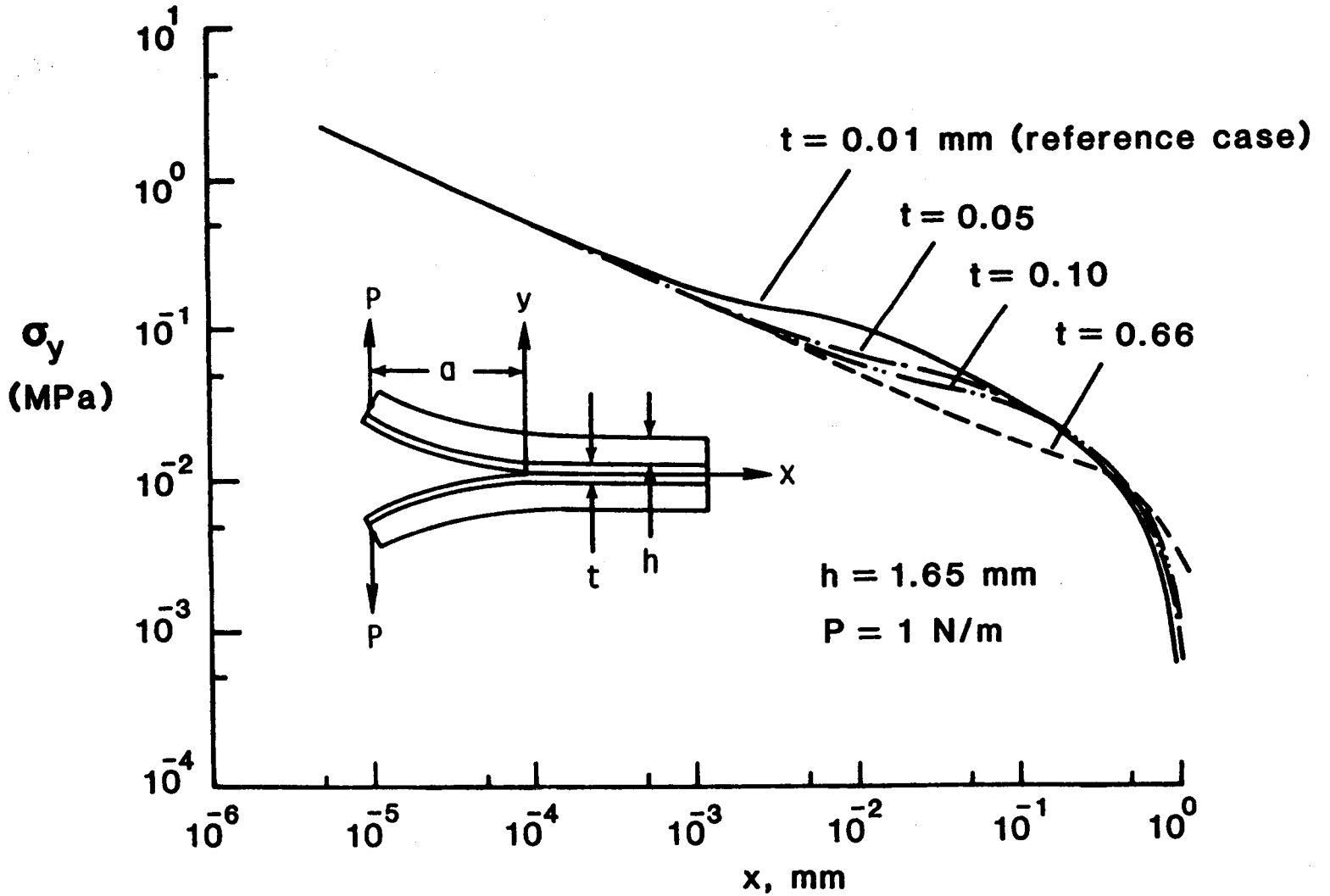

Figure 8.- Effect of adhesive thickness in graphite/epoxy DCB specimen.

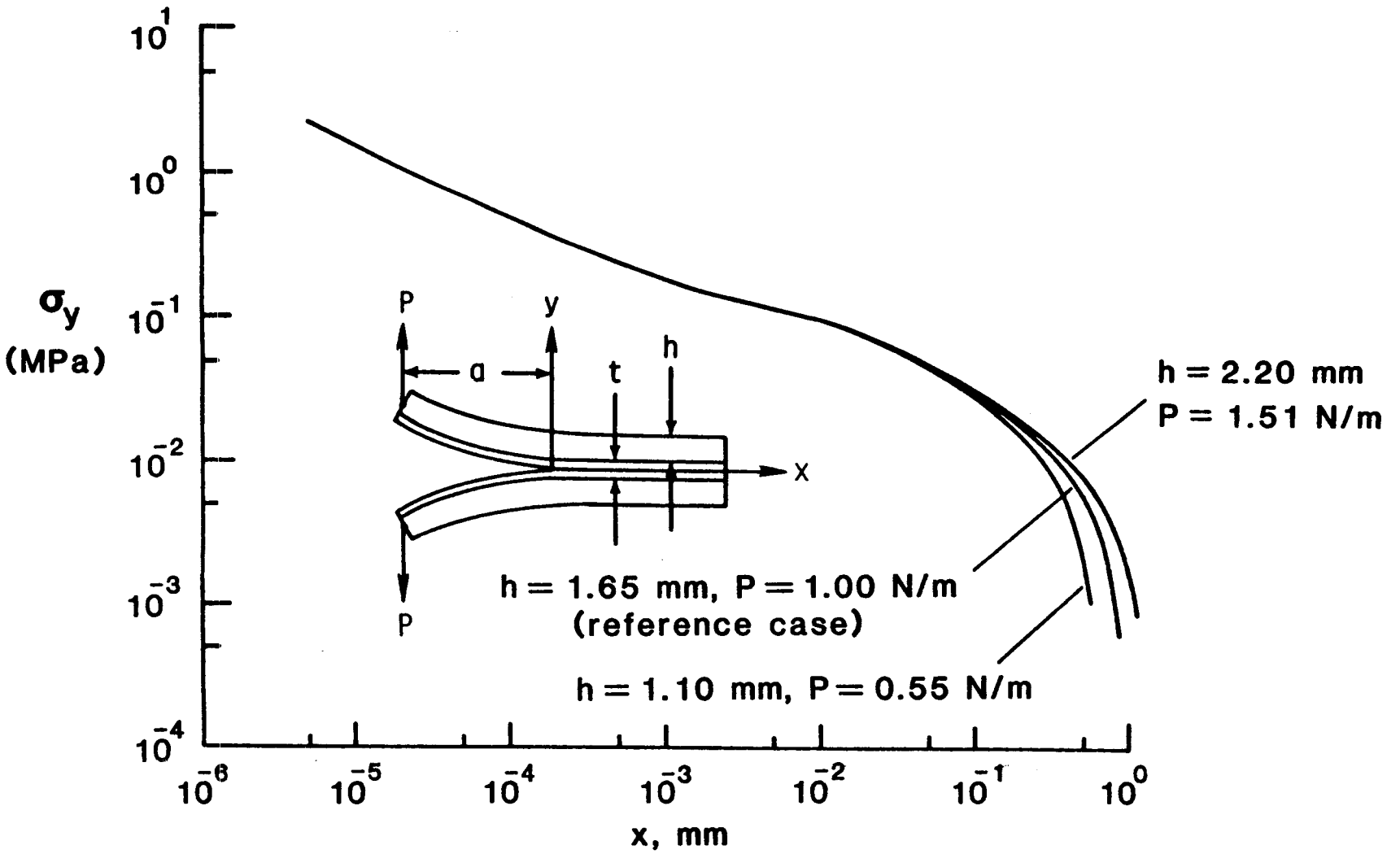

Figure 9.- Effect of adherend thickness in graphite/epoxy DCB specimen.

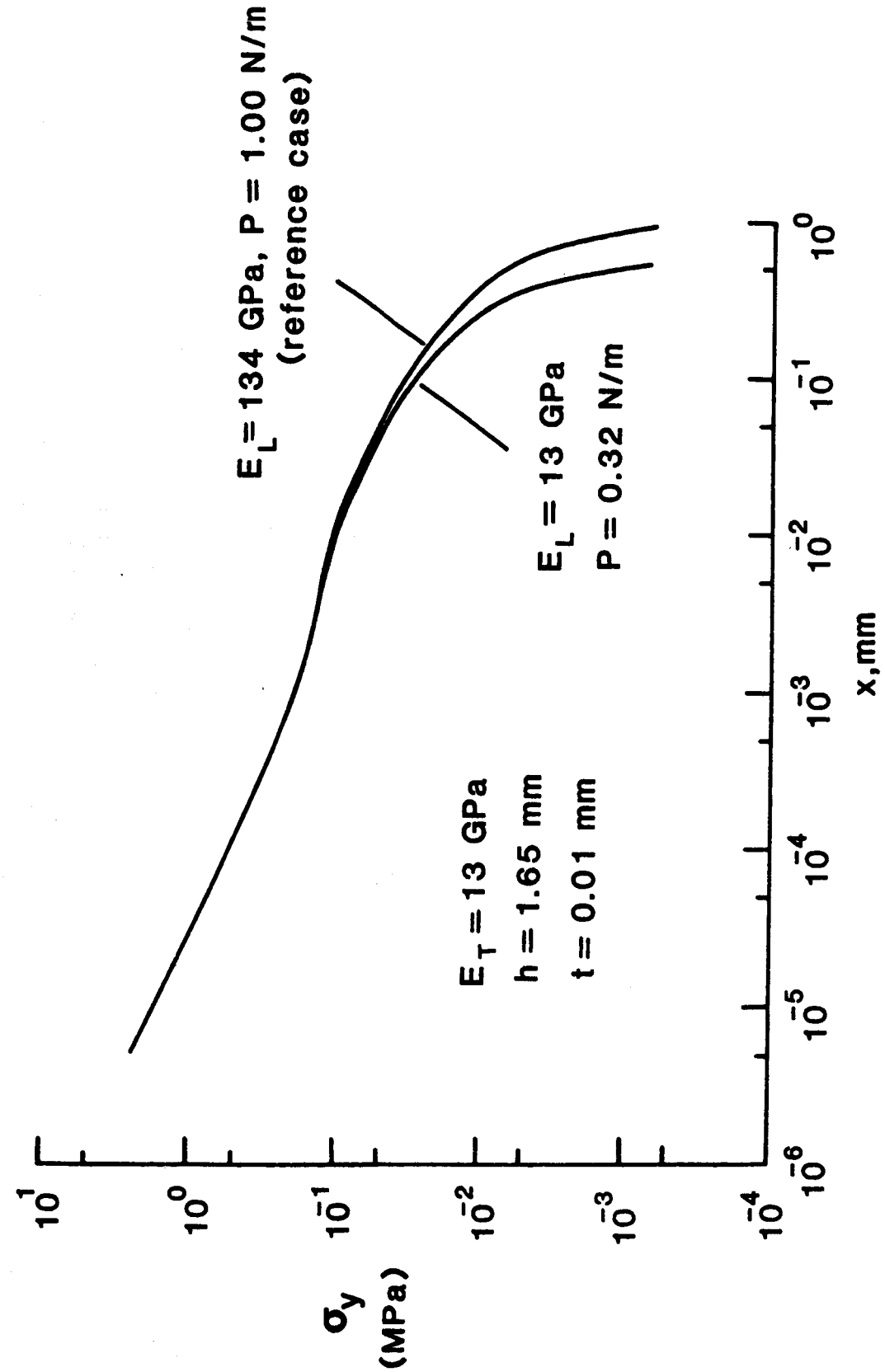

Figure 10.- Effect of adherend longitudinal stiffness.

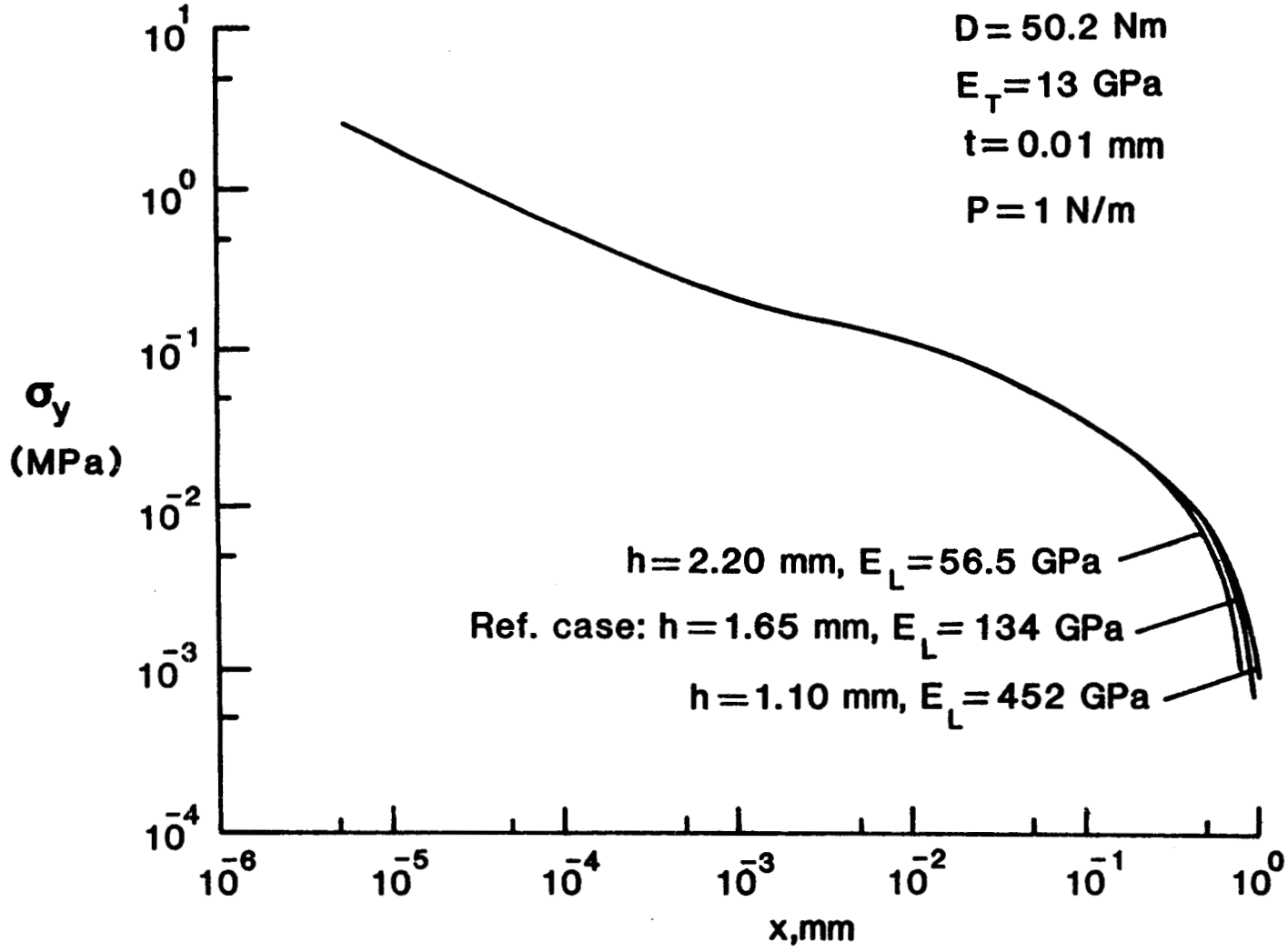

Figure 11.- Stress distributions for constant flexural stiffness.

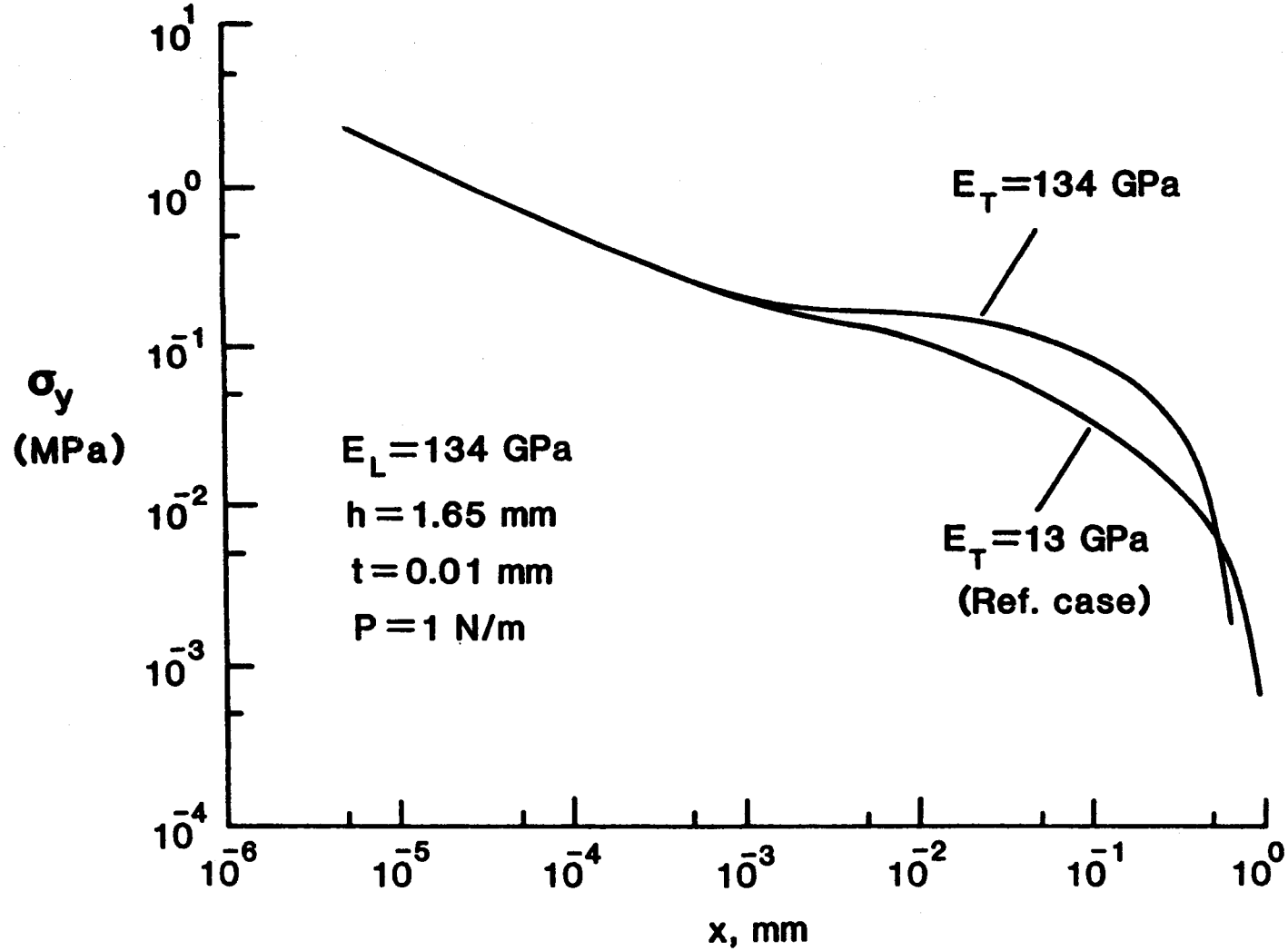

Figure 12.- Effect of adherend transverse stiffness.

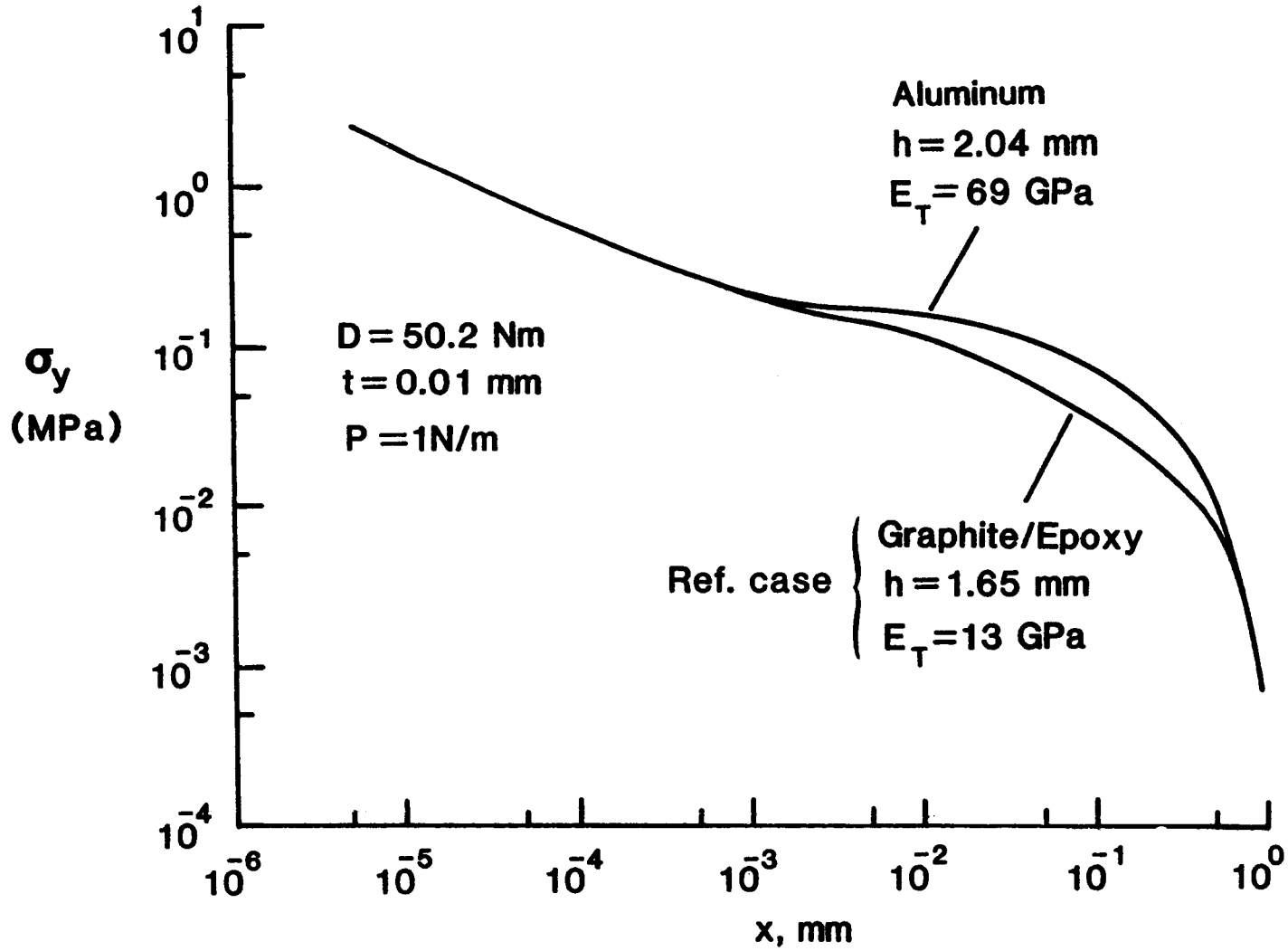

Figure 13.- Comparison of aluminum and graphite/epoxy specimens with the same flexural stiffness.

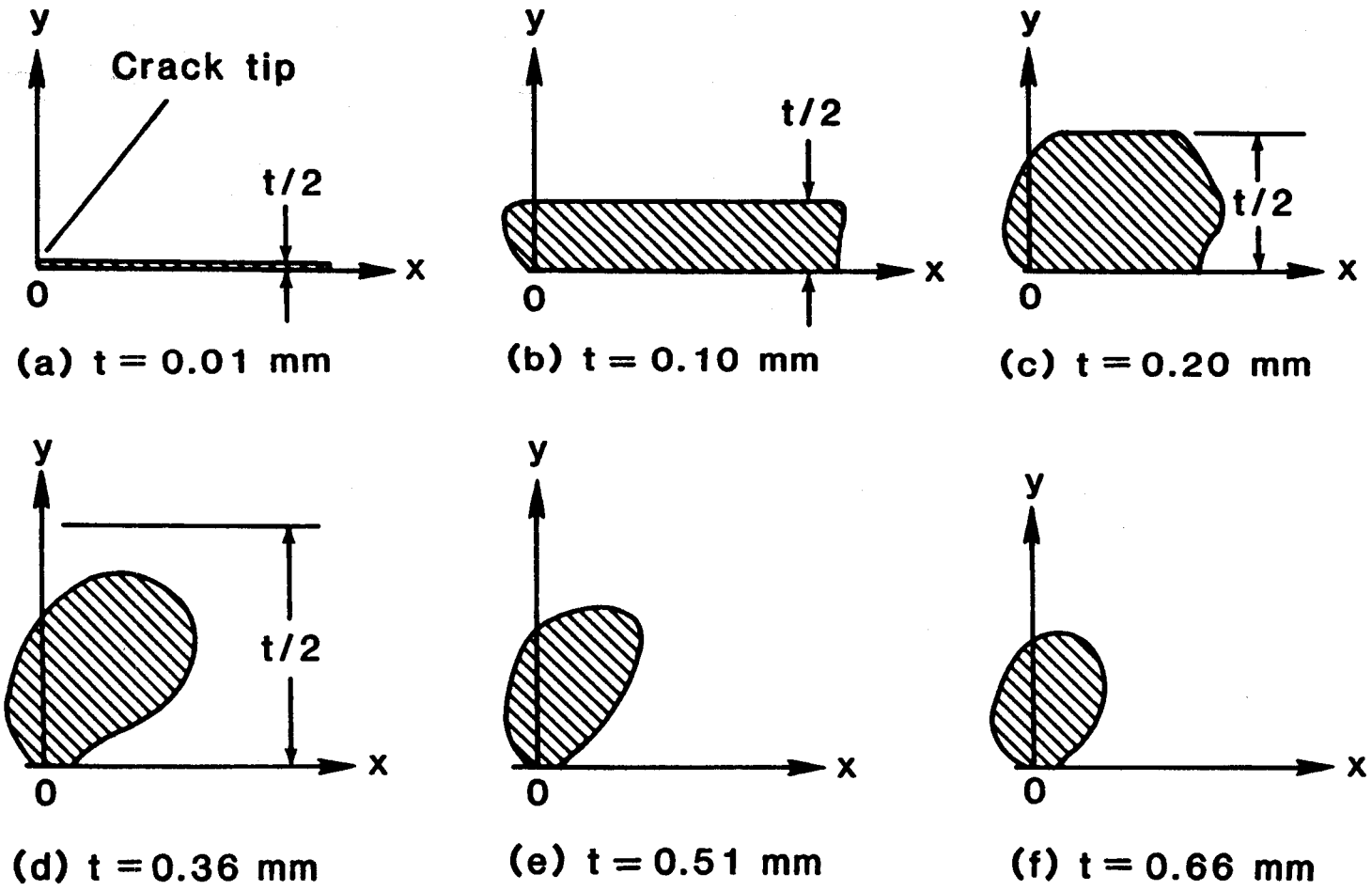

Figure 14.- Yield zones for a range of adhesive thicknesses, aluminum DCB, K_I = 1.18 $MN/m^{3/2}$, h = 1.65 mm.

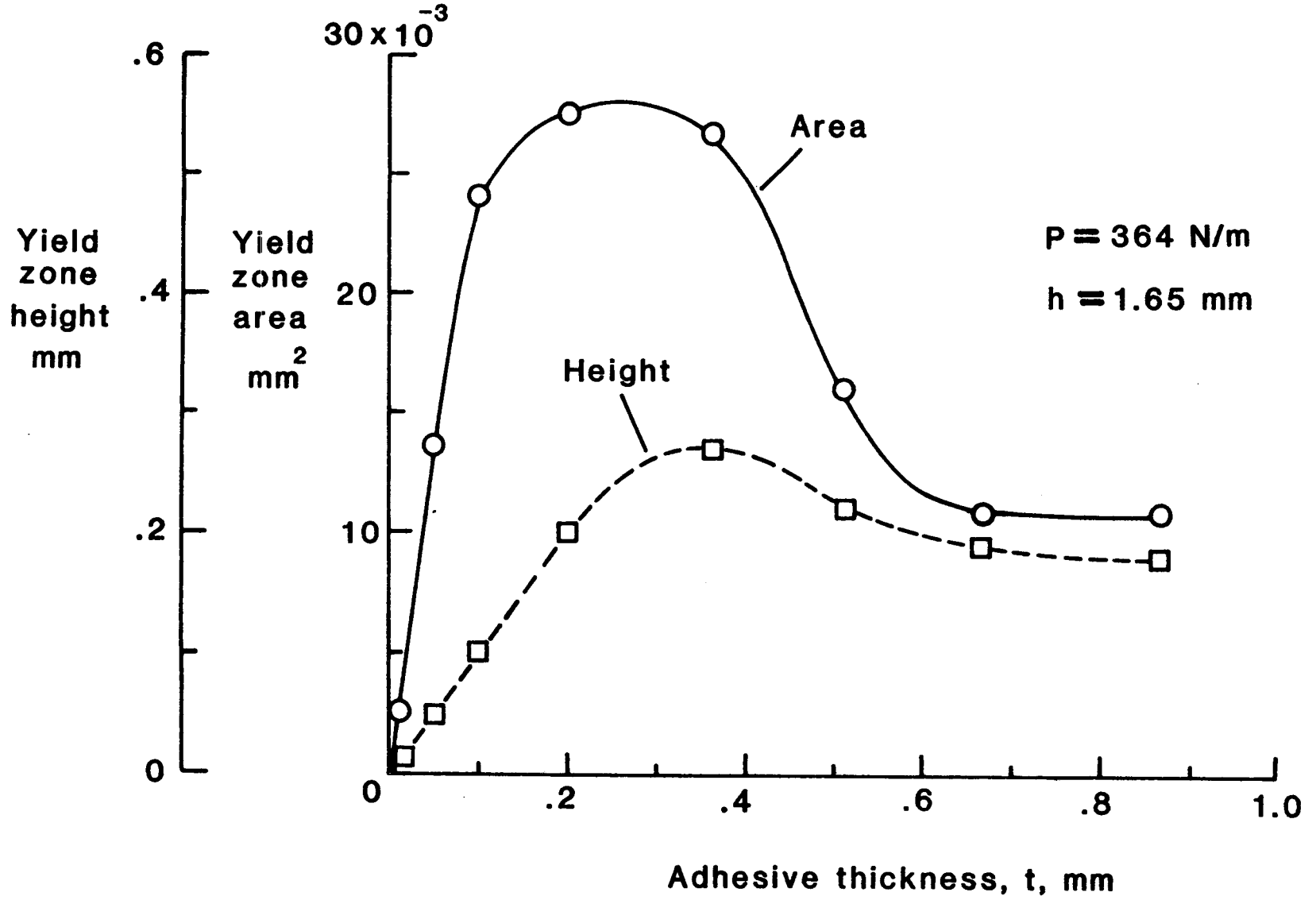

Figure 15.- Yield zone area and height for aluminum DCB specimen.

Standard Bibliographic Page

1. Report No.	2. Government Accession No.	3. Recipient's Catalog No.
NASA TM-89033		

4. Title and Subtitle	5. Report Date
Factors Influencing Elastic Stresses in Double Cantilever Beam Specimens	November 1986
	6. Performing Organization Code: 506-43-11-04
7. Author(s): J. H. Crews, Jr., K. N. Shivakumar and I. S. Raju	8. Performing Organization Report No.
9. Performing Organization Name and Address: NASA Langley Research Center, Hampton, VA 23665-5225	10. Work Unit No.
	11. Contract or Grant No.
12. Sponsoring Agency Name and Address: National Aeronautics and Space Administration, Washington, DC 20546	13. Type of Report and Period Covered: Technical Memorandum
	14. Sponsoring Agency Code

15. Supplementary Notes

*K. N. Shivakumar and I. S. Raju, Analytical Services and Materials, Inc., Hampton, VA 23666

16. Abstract

An elastic stress analysis was conducted for a double cantilever beam (DCB) specimen using finite-element methods. The purpose of this study was to identify the important parameters that influence stresses ahead of the delamination front. The study focused on an aluminum DCB specimen, typical of adhesively-bonded joints, and on a graphite/epoxy specimen representing a cocured composite. Opening mode σ_y stresses ahead of the crack tip were calculated and compared with those for a monolithic reference specimen. Beyond the singularity-dominated region very near the crack tip, the σ_y distribution was elevated compared to the monolithic case. Both the adhesive thickness and the adherend transverse (thickness-direction) stiffness were found to influence the elevation of σ_y. In contrast, adherend thickness and longitudinal stiffness had very little effect on this stress distribution. Estimates for adhesive yielding beyond the aluminum DCB crack tip showed that both the area and height of the plastic zone increased to a peak value for increasing adhesive thicknesses. Results from this study would provide insight for comparing data from different DCB specimens and for designing new DCB specimens.

17. Key Words (Suggested by Authors(s))	18. Distribution Statement
DCB specimen Crack tip Elastic properties Yield zone Stress distributions	Unclassified - Unlimited Subject Category - 39

19. Security Classif.(of this report)	20. Security Classif.(of this page)	21. No. of Pages	22. Price
Unclassified	Unclassified	33	A02

For sale by the National Technical Information Service, Springfield, Virginia 22161